Applied Surface Science 258 (2012) 8273–8278

Contents lists available at SciVerse ScienceDirect

Applied Surface Science

journal homepage: www.elsevier.com/locate/apsusc

Corrosion behavior of chromium and oxygen plasma-modified magnesium in sulfate solution and simulated body fluid

Ruizhen Xu[a], Guosong Wu[a], Xiongbo Yang[a], Xuming Zhang[a], Zhengwei Wu[a], Guangyong Sun[b], Guangyao Li[b], Paul K. Chu[a,*]

[a] Department of Physics and Materials Science, City University of Hong Kong, Tat Chee Avenue, Hong Kong, China
[b] State Key Laboratory of Advanced Design and Manufacturing for Vehicle Body, Hunan University, Changsha 410082, China

ARTICLE INFO

Article history:
Received 2 March 2012
Received in revised form 4 May 2012
Accepted 7 May 2012
Available online 11 May 2012

Keywords:
Magnesium
Ion implantation
Corrosion resistance

ABSTRACT

Because of the unique mechanical properties and biocompatibility, magnesium and its alloys have large potential as lightweight structural materials in the industry in addition to being naturally degradable and resorbable biomaterials. However, their corrosion resistance is usually inadequate especially in an aqueous environment. In this work, pure magnesium is implanted with chromium and oxygen by plasma immersion ion implantation (PIII) and the corrosion behavior is systematically investigated in simulated body fluid and sodium sulfate solution by polarization tests and electrochemical impedance spectroscopy. Our results reveal that chromium and oxygen ion-implanted magnesium have a lower corrosion rate and exhibit less pitting corrosion in the two solutions.

1. Introduction

As lightweight structural materials, magnesium and its alloys have large potential in the aerospace, automotive, and mobile electronics industry [1,2]. Concurrently, magnesium and its alloys have attracted much attention due to their superior specific strength and natural biodegradable properties which are attractive for stents and orthopedic implants. These biomedical implants can degrade naturally and do not require a second surgery to remove them after tissues have healed sufficiently [3]. However, the poor corrosion resistance, especially in an aqueous environment, restricts their application and protection from corrosion remains a critical issue hindering practical applications.

Plasma immersion ion implantation (PIII) is an effective and efficient 3-dimensional surface modification technique [4,5] via ion implanting and formation of graded near-surface structures. Recent studies on implantation of metal ions such as Al [6,7], Ti [7–9], Ta [10], Y [11], Ce [12], and Zr [7] reveal that the implanted Mg alloys exhibit certain degrees of corrosion resistance enhancement in different test solutions. A more compact surface oxide layers can be formed by N [13] and H_2O [14] ion implantation leading to higher corrosion resistance. The corrosion resistance of Mg alloys can also be improved by implanting O [15], H [16], or hydrocarbons such as methane and acetylene [17]. Owing to galvanic effects, the corrosion rates of Mg alloys are accelerated after Zn [18,19] or Cr [20] ion implantation. In contrast, the corrosion rate can be retarded by first implanting Cr followed by oxygen [20]. However, the corrosion behavior and intrinsic mechanism have not been studied systematically.

In this work, the PIII process is optimized and the corrosion behavior and mechanism are investigated systematically in two different environments. To better understand the corrosion behavior of magnesium before and after chromium and oxygen ion implantation, both simulated body fluid (SBF) and 0.1 mol/l sodium sulfate are used in the electrochemical tests (polarization tests and electrochemical impedance spectroscopy). After the immersion tests for different durations, the corrosion products are analyzed by scanning electron microscopy (SEM), energy-dispersive X-ray spectroscopy (EDS), and X-ray photoelectron spectroscopy. The associated corrosion mechanism is also discussed.

2. Experimental details

The materials were as-cast pure magnesium blocks (99.95% pure; 10 mm × 10 mm × 5 mm) mechanically polished using up to 1 μm alumina powder and ultrasonically cleaned in ethanol. The samples were implanted with chromium ions and then oxygen ion implantation was conducted afterwards. Chromium ion implantation was carried out on the HEMII-80 ion implanter equipped with a chromium cathodic arc source. The samples were implanted for 0.5 h at an accelerating voltage of 15 kV and base pressure of 10^{-4} Pa. Oxygen ion implantation was performed on the GPI-100

* Corresponding author.
E-mail address: paul.chu@cityu.edu.hk (P.K. Chu).

0169-4332/$ – see front matter © 2012 Elsevier B.V. All rights reserved.
http://dx.doi.org/10.1016/j.apsusc.2012.05.036

ion implanter. An oxygen plasma was first formed in the chamber at an oxygen flow rate of 20 sccm. A pulsed voltage of 30 kV with a pulse width of 50 μs and pulsing frequency of 100 Hz was applied to the samples and oxygen plasma immersion ion implantation (PIII) was conducted for 3 h.

The Mg, Cr, and O depth profiles were acquired by X-ray photoelectron spectroscopy (XPS) on the Physical Electronics PHI 5802. Al K_α irradiation was employed to determine the chemical states and the estimated sputtering rate was 6.9 nm/min.

The simulated body fluid (SBF) was prepared with deionized water. The concentrations (mmol/l) of the various ions in the SBF were: 142.0 Na^+, 5.0 K^+, 1.5 Mg^{2+}, 2.5 Ca^{2+}, 147.8 Cl^-, 4.2 HCO_3^-, 1.0 HPO_4^{2-}, 0.5 SO_4^{2-}. A 1 mol/l HCl solution was pipetted to adjust the pH to 7.25 at 37 °C. The other electrolyte was 0.1 M Na_2SO_4.

The electrochemical corrosion behavior of the implanted magnesium and pure magnesium were studied on a Zennium electrochemical workstation. The samples were encapsulated by silicone so that only an area of 10 mm × 10 mm was exposed to 80 ml of the test solutions. Potentiodynamic polarization tests and electrochemical impedance spectroscopy (EIS) were conducted in a standard electrochemical cell using three electrodes. The sample was the working electrode. A saturated calomel electrode (SCE) was used as a reference electrode and a platinum electrode served as the counter electrode. The SBF was placed in a water bath at 37 °C and the test in the Na_2SO_4 solution was performed at about 22 °C. The polarization tests were conducted at a scanning rate of 1 mV s^{-1} and EIS were conducted from 100 mHz to 100 kHz. To evaluate the corrosion behavior systematically, the implanted magnesium and pure magnesium samples were immersed in the two solutions for 3 h and 18 h. The temperature of the SBF was kept at 37 °C in a water bath and the Na_2SO_4 solution was kept at about 22 °C. The morphology and microstructure of the corroded surfaces were examined using the Canon EOS 600D Digital SLR camera (DC) coupled with scanning electron microscopy (SEM, FEI/Philips XL30 Esem-FEG). The chemical state of the corrosion product was identified by XPS and energy-dispersive X-ray spectroscopy (EDS, JEOL SM820).

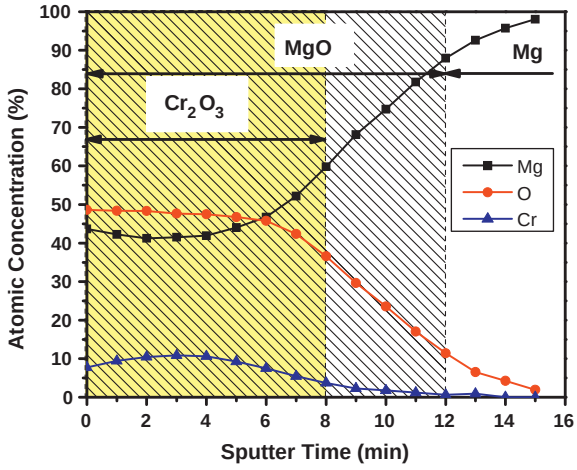

Fig. 1. XPS depth profiles of the implanted sample.

3. Results and discussion

The XPS depth profiles obtained from the implanted sample depicted in Fig. 1 confirm that Cr has a Gaussian-type distribution with a peak concentration of about 10 at%. The O concentration does not change much in the beginning but decreases quickly afterwards whereas the Mg concentration increases gradually as the concentrations of the implanted elements diminish in depth.

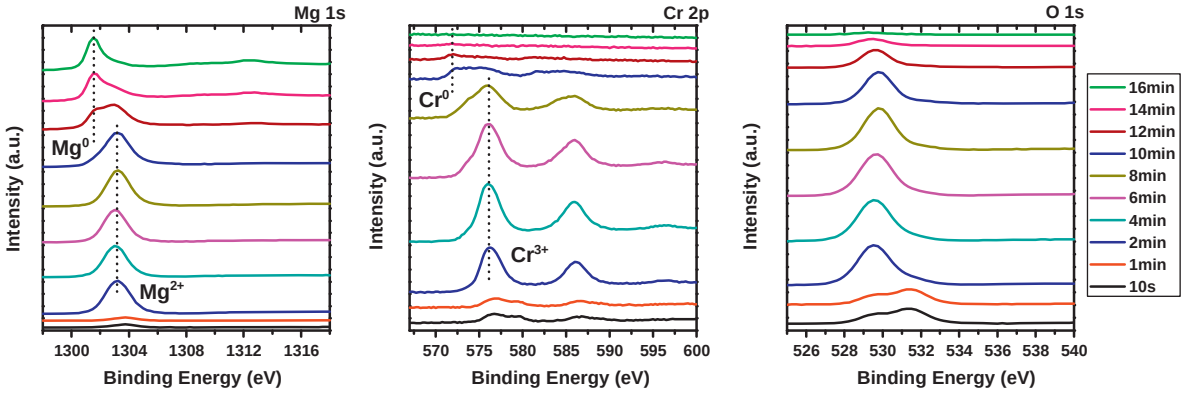

Fig. 2. High-resolution XPS spectra of the implanted sample.

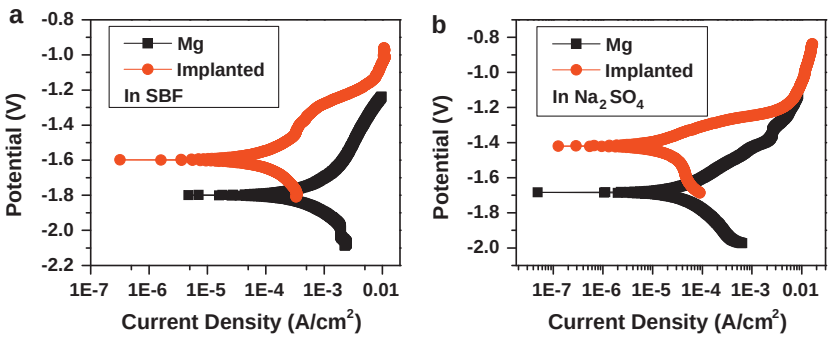

Fig. 3. Polarization curves of Mg and implanted samples in: (a) SBF and (b) Na_2SO_4 solution.

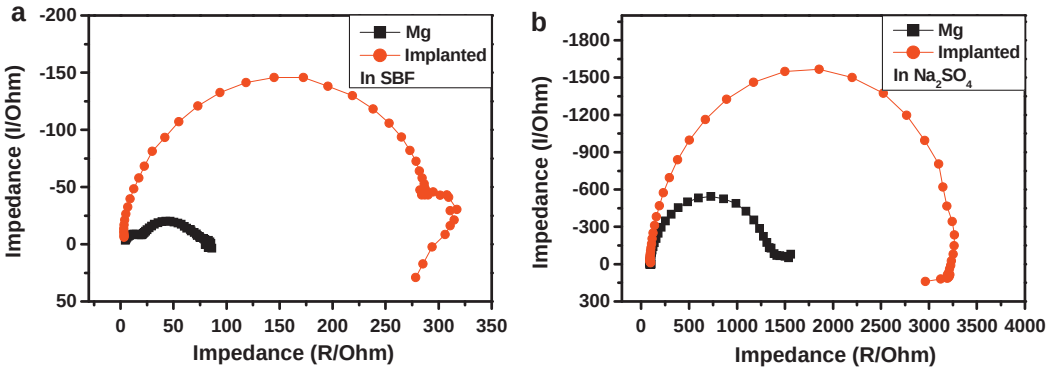

Fig. 4. Typical electrochemical impedance spectra of Mg and implanted samples immersed in (a) SBF and (b) Na_2SO_4 solution.

Fig. 2 presents the high-resolution XPS spectra of Mg 1s, O 1s, and Cr 2p acquired from the implanted sample. With sputtering, the Mg 1s peak shifts from the oxidized state (Mg^{2+}) in the near surface to the metallic state (Mg^0). The Cr 2p peak indicates that almost all the Cr is oxidized (Cr^{3+}). The data disclose that an oxide layer (MgO, Cr_2O_3) is present on the surface of the implanted sample as observed independently in Fig. 1 [18].

The potentiodynamic polarization results obtained in the different solutions are presented in Fig. 3. The corrosion potentials (E_{corr}) of pure Mg and implanted magnesium in SBF are −1.7998 V and −1.5983 V, respectively. In the sodium sulfate solution, the corrosion potential of pure Mg is −1.684 V and that of implanted magnesium is −1.420 V. Compared to the untreated sample, the corrosion potentials of the implanted Mg are enhanced by 201 mV in SBF and 264 mV in sodium sulfate. Larger negative E_{corr} values indicate a more cathodic behavior [21]. According to the cathodic region of the curves, the corrosion current densities of the implanted Mg (1.34×10^{-4} A/cm^2) in SBF is smaller than that of Mg (4.77×10^{-4} A/cm^2), meaning that the implanted sample has better corrosion resistance in SBF [20]. The corrosion current densities of the unimplanted and implanted samples in sodium sulfate are 6.65×10^{-4} A/cm^2 and 2.32×10^{-4} A/cm^2, respectively, also indicating that the implanted sample is more stable in the Na_2SO_4 solution. Similar results are obtained from the EIS and immersion tests and will be discussed later.

EIS is a powerful technique to study the electrochemical reactions and associated mechanism. When an excitation signal with a small amplitude is applied to the system, the response depends on the electrode kinetics. It usually consists of several subprocesses such as mass transfer, charge transfer, and so on. By analyzing these responses, the individual processes can be deduced [22,23]. Fig. 4 shows the Nyquist diagrams of the Mg and implanted samples in SBF and Na_2SO_4 solution. In SBF, the Mg spectrum exhibits a capacitive loop at high frequencies. The Nyquist plot of the implanted sample shows two loops, a capacitive one at high frequencies and an inductive one at low frequencies. In the Na_2SO_4 solution, both the Mg and implanted sample show two loops, a capacitive loop at high frequencies and an inductive one at low frequencies. In the two simulated solutions, the capacitive loops of the implanted samples are enlarged compared to Mg, indicating that they have higher corrosion resistance [24]. In the high frequency range, there is usually a capacitive loop in the Nyquist plots caused by the non-Faradaic electrochemical reaction process. The inductive loop is attributed mainly to the partially protective film resulting in pitting corrosion [22]. These results are confirmed by the immersion tests.

In order to explore the corrosion mechanism in more details, the untreated sample and treated samples are immersed into SBF at 37 °C and Na_2SO_4 solution at room temperature (about 22 °C) for 3 h and 18 h. Afterwards, the samples are carefully analyzed using a digital camera (DC) and SEM. The morphological images of the different samples immersed in sodium sulfate are displayed in Fig. 5. The DC images (Fig. 5a and c) reveal that the Mg is totally corroded but the implanted sample is almost intact with the exception of some small dots with white corrosive products after immersion for 3 h. When the immersion time is extended to 18 h, some marks not noticeable to the naked eyes after immersion for 3 h appear (Fig. 5b) and white corroded dots can be found on the implanted sample (Fig. 5d). Fig. 5a-2 shows that the size is about 10 μm. Fig. 5c-1 and d-1 discloses that the diameter of the pitting corrosion products changes from less than 500 μm after immersion for 3 h to more than 500 μm after immersion for 18 h. Pitting corrosion is confirmed by EIS and corrosion is more serious when the duration is extended. The high resolution SEM image in Fig. 5a-3 supports the proposed corrosion mechanism in Na_2SO_4 [25,26]. A primary film of MgO is formed upon exposure to air after polishing. The oxide forms soluble species in an aqueous medium and a $Mg(OH)_2$ film precipitates gradually impeding the corrosion process. The composition of the corrosion products is determined by XPS and will be discussed later in Fig. 6. As the reaction proceeds, the magnesium hydroxide film becomes denser as shown in Fig. 5b-3. Similar results are observed from the corrosion morphology of the implanted samples in Fig. 5c-3 and d-3. In the initial reaction, the morphology is flake-like but as the reaction proceeds, the morphology turns into thick rods thus increasing the surface area to impede the reaction. When the reaction rate is sufficiently reduced, a balance is reached between the formation and dissolution of $Mg(OH)_2$ and a constant thickness results [26].

The corrosion characteristics of the implanted magnesium are governed by the corrosion reactions on individual component phases. The dual Cr and O implanted magnesium sample has a passivating chromium oxide layer and magnesium oxide film on the surface. The chromium oxide film is inactive in an aqueous environment thus providing high corrosion resistance for the implanted magnesium. However, this chromium oxide film has some local defects and is only partially protective. In order to enhance our basic understanding, the corrosion mechanism of magnesium is important [27]. The overall corrosion reaction is [1,28]:

$$Mg + 2H_2O \rightarrow Mg(OH)_2 + H_2 \quad (1)$$

This overall reaction may be expressed as the sum of the following subreactions:

$$Mg \rightarrow Mg^{2+} + 2e^- \text{ (anodic reaction)} \quad (2)$$

$$2H_2O + 2e^- \rightarrow H_2 + 2OH^- \text{ (cathodic reaction)} \quad (3)$$

$$Mg^{2+} + 2OH^- \rightarrow Mg(OH)_2 \text{ (product formation)} \quad (4)$$

The MgO layer on the surface is hydrated during exposure to an aqueous environment [29] which converts the MgO into larger

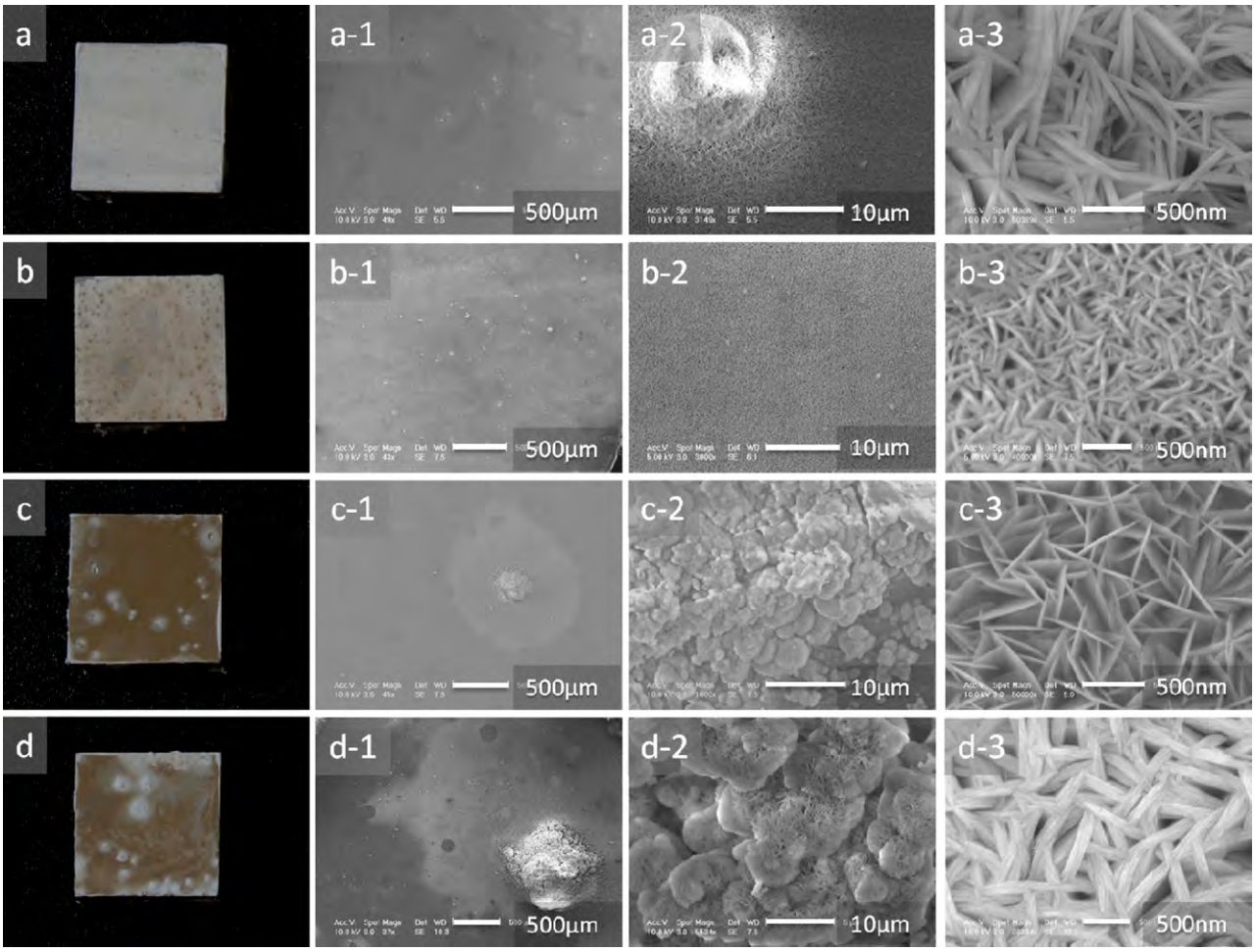

Fig. 5. Morphological images of different samples immersed into Na_2SO_4 solution: (i) digital camera pictures, (i-1) low-magnification SEM pictures and (i-2) medium-magnification SEM pictures, and (i-3) high-magnification SEM [i = a, b, c, and d denoting Mg-3h, Mg-18, implanted-3h, and implanted-18h].

$Mg(OH)_2$. The increased corrosion product volume disrupts the film forming charge instability regions [30]. Compressive ruptures can take place resulting in continuous exposure of the fresh surface. Until dissolution of Mg exceeds the limited solubility, $Mg(OH)_2$ is formed in precipitation.

The overall corrosion reaction of the implanted sample is reasonable in that it is similar to that on pure magnesium. Song et al. [31,32] have shown that Mg is the main component dissolving in the solution during the corrosion reaction of Mg alloys. Moreover, almost no Cr ion is detected from the solution. Hence, it is suggested that in the implanted sample, the above four equations and hydration of MgO are responsible for the corrosion processes taking place in the defective areas in the chromium oxide layer.

As shown in Fig. 6, the amount of hydroxide is significantly greater than those of other products, indicating that the main corrosion product of Mg after immersion in Na_2SO_4 is $Mg(OH)_2$. The O 1s peak on the surface corresponds to oxygen in magnesium hydroxide and magnesium carbonate. At a depth of 50 nm, the O 1s peak corresponds to oxygen in magnesium oxide, magnesium hydroxide, and magnesium carbonate. In a deeper region, the intensity of the magnesium carbonate peak decreases and a magnesium oxide peak emerges. Liu et al. [29] and Bouvier et al. [33] have

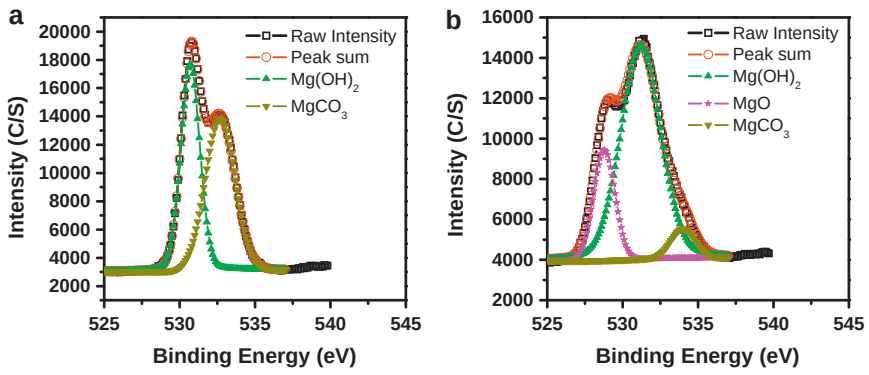

Fig. 6. Fitted curves of the O 1s XPS spectra obtained from Mg after immersion in Na_2SO_4 solution: (a) surface and (b) at a depth of 50 nm.

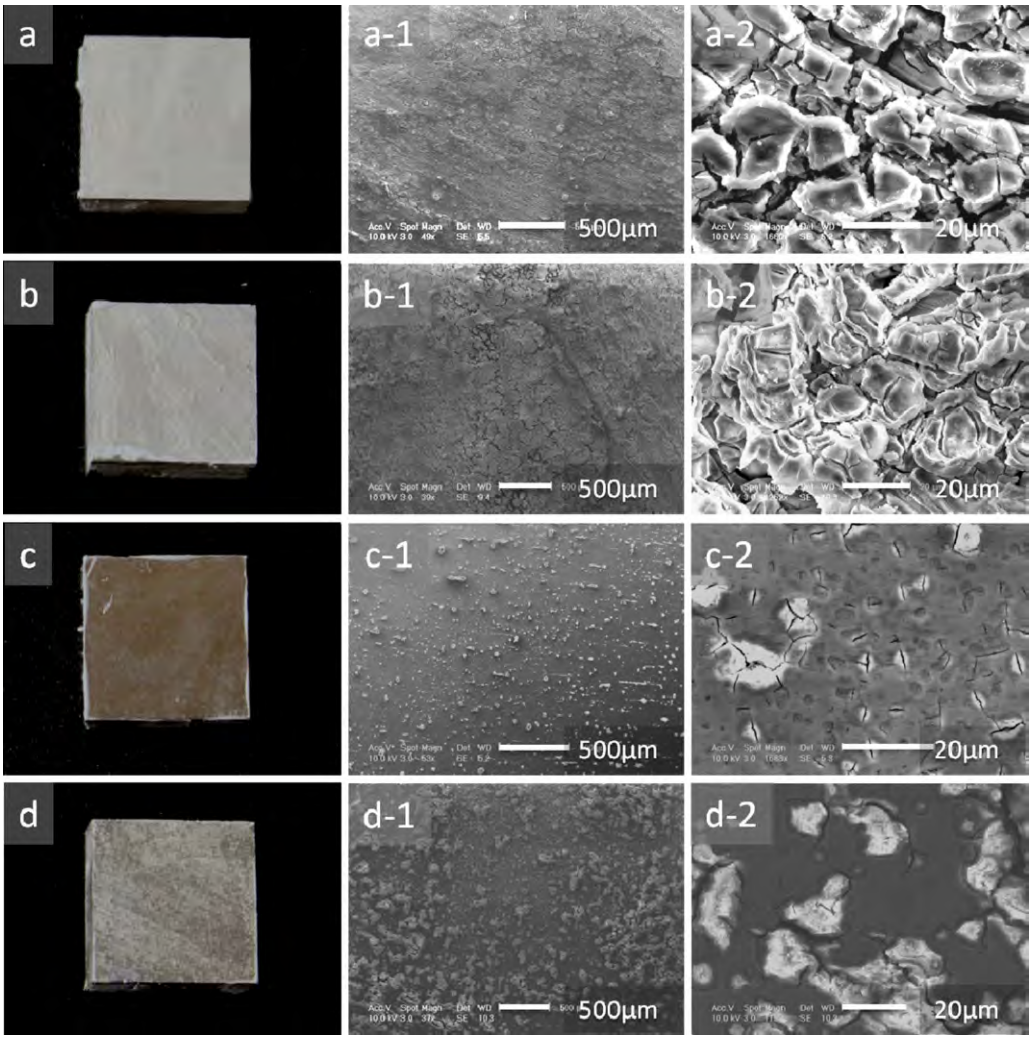

Fig. 7. Morphological images of different samples immersed into SBF: (i) digital camera pictures, (i-1) low-magnification SEM pictures, and (i-2) medium-magnification SEM pictures [i = a, b, c, and d denoting Mg-3h, Mg-18, implanted-3h, and implanted-18h].

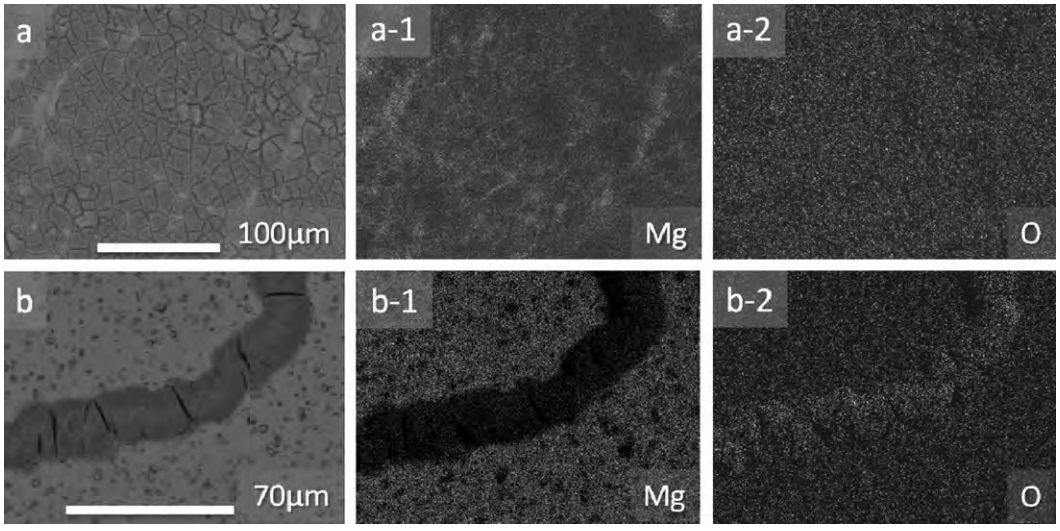

Fig. 8. Elemental maps of Mg and O on different samples after immersion in SBF: (i) SEM images, (i-1) Mg elemental maps, and (i-2) O elemental maps [i = a and b denoting pure Mg and implanted sample].

also observed the appearance of MgO and $MgCO_3$ in the corrosion product of Mg. The MgO and $MgCO_3$ may form during exposure to air.

According to the DC images in Fig. 7a, after immersion in SBF for 3 h, the surface of Mg is fully corroded and covered by white corrosion products. When the time is extended to 18 h, there is no significant difference. The magnified SEM images in Fig. 7a-2 and b-2 reveal a cracked morphology. When the implanted sample is immersed into SBF for 3 h, no distinct corrosion can be seen from Fig. 7c and only small cracks and corrosion products can be found from Fig. 7c-2. As the immersion time is prolonged to 18 h, the partially corroded surface (Fig. 7d) is visible to the naked eyes. The SEM images in Fig. 7d-1 and d-2 show more corrosion products and larger cracks, but some parts of the surface are still intact. The pitting corrosion morphology observed from the implanted magnesium in sodium sulfate is in good agreement with the EIS results.

Compared to Na_2SO_4, SBF has more aggressive ions, especially Cl^-. Staiger et al. [3] have shown that Cl^- not only dissolves the loose film of $Mg(OH)_2$, but also corrodes the Mg substrate directly. The corrosion reactions are as follows [1,34,35]:

$$Mg(OH)_2 + 2Cl^- \rightarrow MgCl_2 + 2OH^- \quad (5)$$

$$Mg + 2Cl^- \rightarrow MgCl_2 \quad (6)$$

Since $MgCl_2$ is soluble in water, it is difficult to detect from the corrosion product. Wang et al. [34] have analyzed the corrosion products on Mg after immersion in SBF by XRD and confirmed that to be mainly $Mg(OH)_2$. Fig. 8 shows the elemental maps of Mg and O on the Mg and implanted sample. The clear patterns of Mg and O in Fig. 8 i-1 and i-2 suggest that the corrosion products are mainly composed of two elements. In SBF, chloride ions can convert the surface $Mg(OH)_2$ into more soluble $MgCl_2$ but they can also penetrate the loose $Mg(OH)_2$ film promoting further dissolution of magnesium. It is a possible reason for the different corrosion products morphology of the $Mg(OH)_2$ in the different solutions.

4. Conclusion

To improve the corrosion resistance of magnesium, dual chromium and oxygen ion implantation is performed on Mg. A protective layer consisting of chromium oxide and magnesium oxide exists on the surface of the implanted samples. The corrosion behavior of the implanted magnesium and pure magnesium is compared in SBF and sodium sulfate by using electrochemical methods and immersion tests. In the electrochemical tests, the corrosion potential increases on the implanted samples and the corrosion current density decreases. In the EIS and immersion tests, owing to local defects on the chromium oxide film, pitting corrosion is the common behavior on the implanted magnesium in both solutions. (The SEM images reveal that the morphology of the corrosion products is different.) The electrochemical and immersion tests demonstrate that the corrosion rates of the implanted sample are lower in both solutions and dual Cr and O ion implantation can effectively retard the surface corrosion reaction on magnesium.

Acknowledgments

This study was supported by Hong Kong Research Grants Council (RGC) General Research Funds (GRF) No. CityU 112510 and the Science Fund of State Key Laboratory of Advanced Design and Manufacturing for Vehicle Body No. 31015007.

References

[1] G.L. Song, A. Atrens, Advanced Engineering Materials 5 (2003) 837–858.
[2] S. Hiromoto, M. Tomozawa, Surface & Coatings Technology 205 (2011) 4711–4719.
[3] M.P. Staiger, A.M. Pietak, J. Huadmai, G. Dias, Biomaterials 27 (2006) 1728–1734.
[4] J.R. Conrad, J.L. Radtke, R.A. Dodd, F.J. Worzala, N.C. Tran, Journal of Applied Physics 62 (1987) 4591–4596.
[5] P.K. Chu, B.Y. Tang, Y.C. Cheng, P.K. Ko, Review of Scientific Instruments 68 (1997) 1866–1874.
[6] M.K. Lei, P. Li, H.G. Yang, X.M. Zhu, Surface & Coatings Technology 201 (2007) 5182–5185.
[7] C.L. Liu, Y.C. Xin, X.B. Tian, P.K. Chu, Thin Solid Films 516 (2007) 422–427.
[8] F. Chen, H. Zhou, S. Cai, F.X. Lv, C.M. Li, Rare Metals 26 (2007) 142–146.
[9] C.G. Liu, Y.C. Xin, X.B. Tian, J. Zhao, P.K. Chu, Journal of Vacuum Science & Technology A 25 (2007) 334–339.
[10] X.M. Wang, X.Q. Zeng, G.S. Wu, S.S. Yao, Y.J. Lai, Journal of Alloys and Compounds 437 (2007) 87–92.
[11] X.M. Wang, X.Q. Zeng, G.S. Wu, S.S. Yao, Materials Letters 61 (2007) 968–970.
[12] X.M. Wang, X.Q. Zeng, S.S. Yao, G.S. Wu, Y.J. Lai, Materials Characterization 59 (2008) 618–623.
[13] X.B. Tian, C.B. Wei, S.Q. Yang, R.K.Y. Fu, P.K. Chu, Surface & Coatings Technology 198 (2005) 454–458.
[14] X.B. Tian, C.B. Wei, S.Q. Yang, R.K.Y. Fu, P.K. Chu, Nuclear Instruments & Methods in Physics Research Section B 242 (2006) 300–302.
[15] G.J. Wan, M.F. Maltz, H. Sun, P.P. Li, N. Huang, Surface & Coatings Technology 201 (2007) 8267–8272.
[16] A. Bakkar, V. Neubert, Corrosion Science 47 (2005) 1211–1225.
[17] M. Yekehtaz, K. Baba, R. Hatada, S. Flege, F. Sittner, W. Ensinger, Nuclear Instruments & Methods in Physics Research Section B 267 (2009) 1666–1669.
[18] G.S. Wu, L. Gong, K. Feng, S.L. Wu, Y. Zhao, P.K. Chu, Materials Letters 65 (2011) 661–663.
[19] Y.Z. Wan, G.Y. Xiong, H.L. Luo, F. He, Y. Huang, Y.L. Wang, Applied Surface Science 254 (2008) 5514–5516.
[20] R.Z. Xu, G.S. Wu, X.B. Yang, T. Hu, Q.Y. Lu, P.K. Chu, Materials Letters 65 (2011) 2171–2173.
[21] W. Zhou, T. Shen, N.N. Aung, Corrosion Science 52 (2010) 1035–1041.
[22] G. Song, A. Atrens, D. St John, X. Wu, J. Nairn, Corrosion Science 39 (1997) 1981–2004.
[23] Y.J. Zhang, C.W. Yan, F.H. Wang, W.F. Li, Corrosion Science 47 (2005) 2816–2831.
[24] G.L. Song, A.L. Bowles, D.H. StJohn, Materials Science and Engineering A 366 (2004) 74–86.
[25] D.A. Vermilyea, C.F. Kirk, Journal of The Electrochemical Society 116 (1969) 1487–1492.
[26] G. Baril, N. Pebere, Corrosion Science 43 (2001) 471–484.
[27] G.L. Song, A. Atrens, Advanced Engineering Materials 1 (1999) 11–33.
[28] G.L. Makar, J. Kruger, International Materials Reviews 38 (1993) 138–153.
[29] M. Liu, S. Zanna, H. Ardelean, I. Frateur, P. Schmutz, G.L. Song, A. Atrens, P. Marcus, Corrosion Science 51 (2009) 1115–1127.
[30] H.B. Yao, Y. Li, A.T.S. Wee, Applied Surface Science 158 (2000) 112–119.
[31] G.L. Song, A. Atrens, X.L. Wu, B. Zhang, Corrosion Science 40 (1998) 1769–1791.
[32] G.L. Song, A. Atrens, M. Dargusch, Corrosion Science 41 (1999) 249–273.
[33] Y. Bouvier, B. Mutel, J. Grimblot, Surface & Coatings Technology 180 (2004) 169–173.
[34] Y. Wang, J. Gao, Y. Zhang, X. Zhou, S. Wu, The Chinese Journal of Nonferrous Metals 17 (2007) 1981–1986.
[35] Y. Xin, T. Hu, P.K. Chu, Acta Biomaterialia 7 (2011) 1452–1459.